Large Eddy Simulation of a Normally Impinging Round Air Jet with Heat Transfer at a Reynolds Number of 4400

Yong-Ping LI[1,a], Qi-Zhao LIN[1,b], Tao-Hong YE[1,c], Zuo-Jin ZHU[2,d,*]

[1]Department of Thermal Science and Energy Engineering, USTC, P.R. China

[2]Faculty of Engineering Science, USTC, P.R. China, Tel: 86-551-3600430

[a]lyplyp@mail.ustc.edu.cn, [b]qlin@ustc.edu.cn, [c]thye@ustc.edu.cn, [d]zuojin@ustc.edu.cn

*Corresponding author

Keywords: Impinging Round Air Jet, Forced Convection, Sub-grid Heat Flux.

Abstract. To explore the heat and fluid flow characteristics of normally impinging round air jet, a large eddy simulation (LES) of the jet flow at a jet-issuing Reynolds number of 4400 for a orifice-to-plate distance equal to five jet nozzle diameters was encompassed using a computer code OpenFoam. A comparison with existing experimental and numerical results was made. It was found that the LES predicted mean Nusselt number is favorably distributed in the radial direction, indicating that the LES has application potential in predicting impinging jet flows at conditions with an increased Reynolds number and a varying orifice-to-plate distance.

Introduction

Impinging jet is used as a conventional method to enhance heat transfer [1, 2]. Increasing the directional and normal velocity gradients and turbulence intensity of fluid flow near the impingement surface can improve the heat transfer [3]. Therefore, the study of impinging round jet with heat transfer is of great significance in engineering application and academics. Before introducing the main objective of this paper, a brief literature review of the impinging jet flow research, which is simply categorized into experimental [3-8] and numerical aspects [8-24] is given below.

The numerical work was done primarily from three aspects: direct numerical simulation (DNS) [9], Reynolds averaged Navier-Stokes (RANS) modeling [10-12], and large eddy simulation (LES) [13-24]. For LES, Olssen and Fuchs [13] numerically predicted a forced semi-confined round impinging jet. For this jet flow, the Reynolds number was 10^4 and the inflow was forced at a Strouhal number of 0.27. The orifice-to-plate distance was four jet-nozzle diameters. They found these secondary vortices are related to the radial deflecting primary vortices generated by the circular shear layer of the jet, the primary vortex structures that reach the wall were helical and not axi-symmetric.

Accompanied by the LES of impinging plane jet flows [14-18], Hällqvist [19] carried out a LES of round impinging air jets with heat transfer. It was found that the top-hat and the turbulent inflow conditions yield a higher rate of incoherent small scale structures. Also the applied level of swirl at the velocity inlet has significant influence on the rate of heat transfer. The turbulence level increases with swirl, which is positive for heat transfer, and so also the spreading of the jet. In 2008, to gain a better insight into flow, Hadžiabdic and Hanjalic [20] reported their LES results of a normally impinging round jet issuing from a long pipe at a Reynolds number Re=2×10^4, and H/D =2. It was found that there exist interesting time and spatial dynamics of the vorticity and eddy structures and their imprints on the target wall.

In 2009, Uddin *et al.* [21] reported the LES results of turbulent round air jets that normally impinge on a target surface, what focused was the case at the relatively high value of Reynolds number of 2.3×10^4 (based on round jet-issuing conditions) for which experimental data are available. They found that only one of the models considered succeeds in representing the effects on the heat fluxes of the complex strain field associated with the stagnation region and the subsequent development into the wall jet region, and discussed the relevant reasons for this outcome.

In 2011, Nicoud *et al.* [22] applied singular values to build a SGS model for LES. They reported that the so-called σ-model has a low computational cost, is easy to implement, and does not require any homogeneous direction in space or time. The results obtained with the proposed model are systematically equivalent or slightly better than the results from the dynamic Smagorinsky model [23].

In 2012, Dewan *et al.* [24] reported the current status of computation of turbulent impinging jet heat transfer. They reviewed the effects of different SGS models, boundary conditions, numerical schemes, grid distribution, and size of the computational domain adopted in various LES of this flow configuration, together with a review of DNS of the same geometry and computation of other complex impinging flows, and a description of some recent attempts in RANS modeling of impinging flows.

More recently, Toda *et al.* [8] have reported a LES-dedicated experiment of a pulsatile hot-jet impinging a flat-plate in the presence of a cold turbulent cross-flow. Two eddy viscosity- based SGS models are investigated: the dynamic Smagorinsky model [23] and the σ-model [22]. It was found both models give similar results during the first phase of the experiment. However, the dynamic Smagorinsky model could not accurately predict the vortex-ring propagation, while the σ-model provides a better agreement with the experimental measurements.

The objective of this paper is to explore the heat and fluid flow characteristics of normally impinging round air jet at a Reynolds number Re= 4400, and *H/D*=5 using LES with dynamic SGS model, mainly because the impinging round air jet flow with heat transfer is an intrinsic thermal fluid flow problem relating to the engineering technology of wall surface ice removing by high temperature round air jet. The LES was done with a computer code OpenFoam. In the LES, it was simply assumed the air jet has the ambient temperature, with the target solid plate wall heating by constant heat flux, as reported [20, 21], because this is more convenient for evaluating the reliability of the LES results. The LES results will be discussed by statistical analysis of turbulence, demonstrating instantaneous flow field, and the comparison with some existing experimental [4, 7] and numerical [20] results.
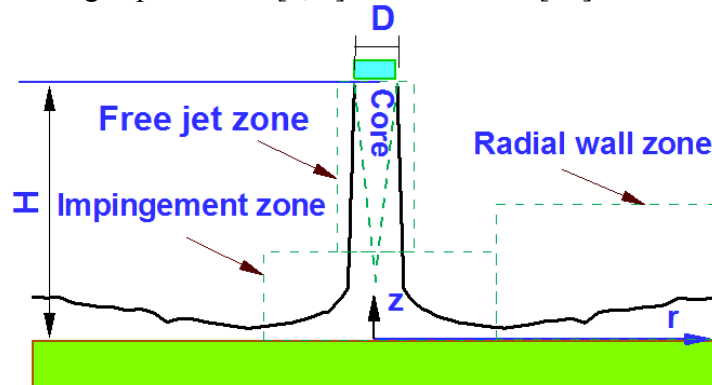

Fig. 1 Schematic of Normally Impinging Round Air Jet

Governing Equations

The heat and fluid flow problem faced by the present LES with the computer code OpenFoam, as schematically shown in Fig. 1, is involved with a round air jet impinging normally to a plat plate, with an orifice-to-plate distance of five times the jet-nozzle diameter, i.e. *H*=5*D*,at a jet-issuing Reynolds number $(Re = W_b D / \nu)$ of 4400, for which the jet impinging flow is turbulent [21]. The flow has a jet core zone, an impingement zone and a radial wall zone. The computer code OpenFoam has the simulation function of possibly satisfying some users' prediction demands through adding some subroutines. For the convenience of prediction, it was assumed that the jet air has a temperature identical to the ambient, but the temperature is lower than that of the plate surface, indicating that the normally impinging round air jet plays a cooling role for the target wall surface. Further, it was assumed that the flow is incompressible, and cooling mode is mainly related to the forced convection, while the contributions due to buoyancy caused natural convection and wall thermal radiation are negligible. Following the published work [12, 21], the governing equations on the basis of the conservations of mass, momentum and energy have the following form

$$\frac{\partial u_i}{\partial x_i} = 0,$$

(1)

$$\frac{\partial u_i}{\partial t} + \frac{\partial \left(u_j u_i \right)}{\partial x_j} = -\frac{1}{\rho}\frac{\partial p}{\partial x_i} + v\frac{\partial}{\partial x_j}\left[\frac{\partial u_i}{\partial x_j} + \frac{\partial u_j}{\partial x_i} \right] - \frac{1}{\rho}\frac{\partial \tau_{ij}^s}{\partial x_j},$$

(2)

$$\frac{\partial \left(c_\rho T \right)}{\partial t} + \frac{\partial \left(c_\rho u_j T \right)}{\partial x_j} = -\frac{1}{\rho}\frac{\partial}{\partial x_j}\left[\Gamma c_\rho \frac{\partial T}{\partial x_j} \right] - \frac{1}{\rho}\frac{\partial q_j^s}{\partial x_j}.$$

(3)

Where $\hat{u}_i$ is the flow velocity component in x_i direction, $\hat{T}$ represents the fluid temperature, with the over hat " ^ " denoting the resolved variables. The sub-grid scale stress is defined by

$$\tau_{ij}^s = \rho\left(u_i u_j - u_i u_j \right).$$

(4)

The sub-grid scale closure models for momentum are based on a gradient-diffusion hypothesis, which can be expressed as a relation between the anisotropic stress and (large-scale) strain rate tensor

$$\tau_{ij}^s - \frac{1}{3}\delta_{ij}\tau_{kk}^s = 2\rho v_s\left(S_{ij} - \frac{1}{3}\delta_{ij}S_{kk} \right),$$

(5)

Where v_s is the sub-grid viscosity, expressed as

$$v_s = \left(c_s\Delta \right)^2 S = \left(c_s\Delta \right)^2 \sqrt{2S_{ij}S_{ij}},$$

(6)

with the resolved strain rate given by

$$S_{ij} = \frac{1}{2}\left(\frac{\partial u_i}{\partial x_j} + \frac{\partial u_j}{\partial x_i} \right).$$

(7)

In Eq. (6), Δ is the grid filter width, c_s is a constant specified by the dynamic Smagorisky model [25]. Note that there are other kind's approaches to assign the sub-grid viscosity, as reported elsewhere [26-32].

The sub-grid heat flux q_j^s is expressed as

$$q_j^s = \rho c_p\left(u_j T - u_j T \right),$$

(8)

Again, using the gradient diffusion assumption similar to Uddin *et al.* [21], let Pr_s be sub-grid Prandtl number, we have

$$q_j^s = -\frac{\rho v_s}{\mathrm{Pr}_s}c_p\frac{\partial T}{\partial x_j},$$

(9)

where ($\rho v_s/\mathrm{Pr}_s$) denotes the sub-grid thermal diffusivity. In the present LES, the sub-grid Prandtl number Pr_s was assigned as 0.85.

The top and side open boundaries were assigned to have constant pressure conditions, which allow the occurrence of possible reverse flow. The inflow turbulence intensity was assumed at the level of 1%, so that the root mean square (RMS) value of velocity fluctuation for each component can be simply set as one percent of W_b. On the target plate wall surface, unmovable condition and constant heat flux condition were given. Similar to the published work [21], the heat flux was set as 1000W/m². While the ambient air

temperature in the present LES was 300K rather than 293K, at which the thermophysical properties of air under standard atmospheric condition were given in Table 1.

Tab. 1 Thermophysical Properties of Air Used in the LES

ρ [kg/m^3]	c_p [kJ/(kg·K)]	k [W/(m·K)]	ν [m^2/s]	Pr
1.1767	1.0066	0.0262	1.58×10^{-5}	0.7196

Numerical Method

The governing equations (1-3) were discretized in an unstructured grid system using control volume approach. The 2nd order Crank-Nicolsen method was used to deal with the temporal gradient term, while the spatial gradients in the nonlinear convective terms was treated with the 2nd order central-differencing scheme. The algebraic equation set were solved by PISO solver.

The time step (Δt) in the LES was code-self adjusted through the use of the Courant number, which should be less than 0.5, i.e. $\Delta t |U| / \delta x < 0.5$, here δx refers to the cell size in the direction of the velocity, and $|U|$ denotes the magnitude of the velocity through that cell. The total cell number is about 1.20×10^6. While the normalized finest grid distance close to the target wall ($z^+ = z u_\tau / \nu$, u_τ denotes friction velocity) is less than 1.87, which causes the time step sometimes should be at the level of micro-second. A grid distribution near the stagnation point was given in Fig. 2. The calculation was encompassed using a single processor at a parallel computation station. Hence it has consumed about three months to output the LES results to be discussed in the next section.
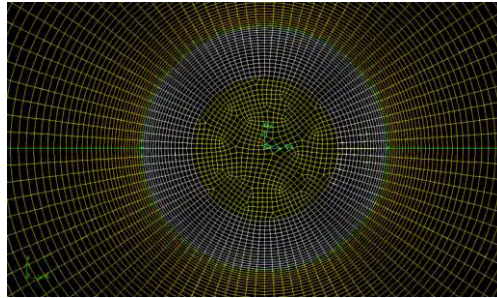

Fig. 2 Grid Distribution near the Staganation Point in the x-y Plane

Results and Discussion

When the jet-nozzle diameter D, and the jet-issuing speed W_b, are taken as the length and speed scales respectively, the time scale t_0 should be D/W_b. In the present LES, D = 0.007m, W_b = 9.93m/s, $t_0 = 7.0493 \times 10^{-3}$ s. For the statistical analysis of the LES results, the time period in the unit of t_0 is $\bar{\tau}$ (≈ 2837), just identical to 2 seconds of real time. It is expected to be sufficiently long to outcome reliable statistic variables, such as the mean values and root mean square values of some heat and fluid flow variables.

A flow field at $t/t_0 = 5801.96$ was shown in Fig. 3, from which, the jet core zone mentioned in Fig. 1 is primarily blue colored, implying that the velocity has a value larger than 8m/s. While in the impingement zone concentrated at the stagnation point, the value of $w(t)$ depends on the spatial position, and in the radial wall zone, the value of $w(t)$ is close to zero but can be positive, reflecting the coherent interaction effect of large vortices near the outer region of impinging caused wall jet layer.

The comparison of velocity components in the vertical direction at two radial positions is illustrated by Fig. 4, where the experimental data labeled by unfilled circle for U/W_b and green-filled diamond for W/W_b were abstracted from Ref. [7] reported by Geers, Tummers and Hanjalic (2004) for the case of H/D=2 at Re=2.3×10^4. Both mean velocity components averaged in the time period of $\bar{\tau}$ (≈ 2837) have

favaroable distribution tendencies in comparison with the measured, the main reason of the observable discrepancies is that the normally impinging round air jet predicted by the present LES has larger orifice to plate distance (*H/D*=5) and lower Reynold number (Re=4400).
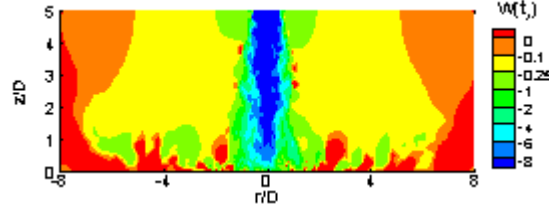

Fig. 3 Instantaneous Flow Field by Velocity Component in the Z-direction at $t/t_0 = 5801.96$

However, the impinging conditions of normally round air jet can also result in the differerent distributions along the vertical direction at different radial positions, as seen in Fig. 5. From Fig. 5(b) for *r/D*=0.5 , it is seen that for despite the apparent discrepancy for the vertical distribution of u_{rms}/W_b, the conststency for the predicted distribution of w_{rms}/W_b is fairly good.
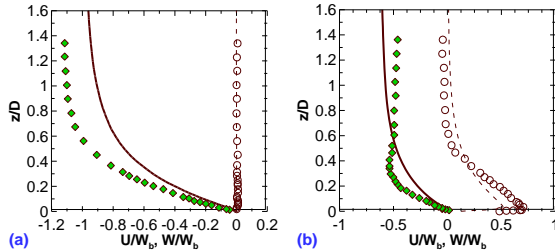

Fig. 4 Comparison of Velocity Component in the Vertical Direction, (a)*r/D* =0; (b)*r/D*=0.5. The data labeled by circle and diamond were from Ref. [7];solid line denotes W/W_b; dashed line represents U/W_b
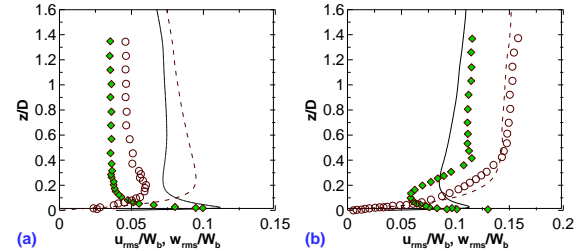
Fig. 5 Comparison of Velocity Fluctuations in the Vertical Direction, (a) *r/D*=0; (b) *r/D* =0.5. The data labeled by circle and diamond were abstracted from Ref. [7]; olid line denotes u_{rms}/W_b, dashed line represents w_{rms}/W_b

On the other hand, the comparison of mean velocity distributions along the radial direction with the numerical results reported by Hadžiabdic and Hanjalic [20] can be seen in Fig. 6(a-b), each part has demonstrated the mean velocity component U/W_b or W/W_b at two distances to the wall surface, i.e. *z/D*=0.0125, 005. In Fig. 6(a), it is seen that the radial velocity distribution is sensitive to *z/D* (the wall distance), for the case of Re=4400, the value of mean velocity U/W_b is larger at *z/D*=0.05 in comparison with that at *z/D*=0.0125, with the mean velocity difference depending on the distance to the impinging jet axis *r/D*. In Fig. 6(b), it is seen that a fairly good agreement with the results reported in Ref. [20] occurs for the wall distance *z/D*=0.05, while for finer wall distance *z/D*=0.0125, there is a large discrepancy. Similarly, we say that the discrepancy in comparison with the numerical results in Ref. [20], which are illustrated by unfilled circle and green-filled diamond, comes from the different jet impinging condition.

The jet impinging condition effect can be seen more obviously from the comparison of subgrid stress, as shown in Fig. 7(a-b). In addition to main features involving with the orifice to plate distance *H/D* and the jet-issuing condition defined Re, the assignment of boundary conditions and the numerical approach can also influence the LES resluts to some extent.

Let the heat transfer coefficient of forced convection be h, the target surface be described by the coordinates $r \ (=\sqrt{x^2 + y^2})$ and $\theta \ [= \arctan(y/x)]$, then if we assume the coefficient was averaged in the θ-direction from zero to 2π, the coefficient can be seen as a single function of coordinate r. Let the adiabatic wall temperature be T_{aw}, for the wall temperature T_w and local heat flux per unit wall area $q_w(r)$, the coefficient can be defined by

$$h = q_w/(T_w - T_{aw}),$$

(10)

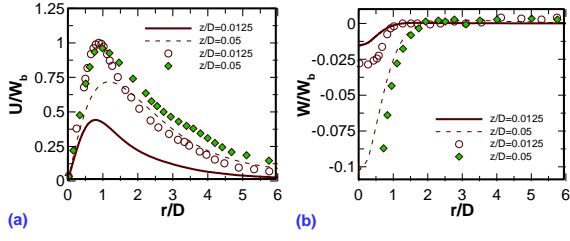Averaging the local Nusselt number

$$Nu = hD / k ,$$ (11)

Fig. 6 Comparison of Mean Velocity Distrinutions along the Radial Direction, (a) U/W_b;(b) W/W_b . The data labeled by unfilled circle and greenfilled diamond were abstracted from the numerical work [20]
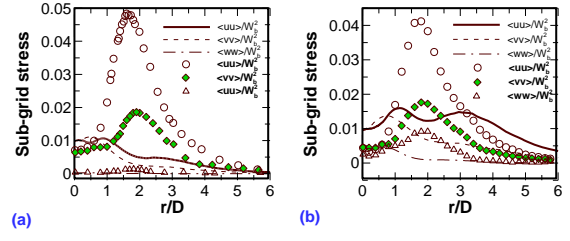

Fig. 7 Comparison of Sub-grid Stress along the Rradial Direction, (a) z/D=0.0125; (b) z/D=0.05. The data labeled by unfilled circle and greenfilled diamond were abstracted from the numerical work [20]

We yield the mean Nusselt number

$$Nu_{av} = \frac{2}{r^2} \int_0^r Nu \cdot r dr ,$$ (12)

As shown in Fig. 8, the predicted values from present LES are found to be favorable in comparison with the data abstracted from Ref. [4]. It is noted that for $r/D \geq 2.5$, the data were calculated by directly using empirical expression
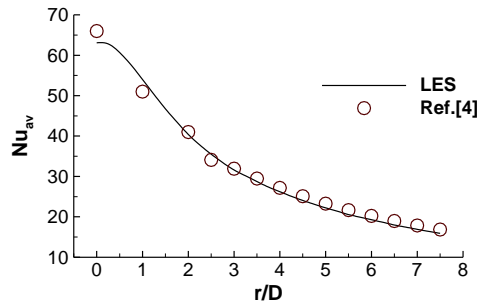

Fig. 8 Nu_{av} as a Function of r/D.

The values of $Nu_{av,\exp}$ lebeled by circles were abstratced from Ref. [4]

$$Nu_{av,\exp} = \frac{\frac{D}{r}(1-1.1\frac{D}{r})}{1+0.1(\frac{H}{D}-6)\frac{D}{r}} \cdot [1.36 \text{Re}^{0.574}\text{Pr}^{0.42}] ,$$ (13)

which is available merely in the Reynolds number range $\text{Re} \in (2000, 30000)$. While for $r/D < 2.5$, data were abstracted with respect to some experimental curves in Ref.[4]. The favaroable comparison of heat transfer confirms that the dynamic LES can be further applied in flows at other impinging conditions, corresponding to varying orifice-to-plate distance and increased jet-issuing condition defined Reynolds number.

Conclusion

A dynamic LES of normally impinging round air jet flow at a jet-issuing Reynolds number of 4400 for a orifice-to-plate distance equal to five jet-nozzle diameters was encompassed to explore the relevant heat and fluid flow characteristics. A favorable agreement for the heat transfer by forced convection was

obtained, indicating that the LES can be further applied to study the impinging round air jet flow at conditions with an increased Reynolds number and a varying orifice-to-plate distance.

Acknowledgement

References

[1]K. Jambunathan, E. Lai, M.A. Moss and B.L. Button, A Review of heat transfer data for single circular jet impingement, Int. J. Heat Fluid Flow 13(1992)106-115.

[2]R. Viskanta, Heat transfer to impinging isothermal gas and flame jets, Exp. Therm. Fluid Sci. 6(1993)111-134.

[3]K. Ichimiya and Y. Yoshida, Oscillation effect of impingement surface on two-dimensional impingement heat transfer, ASME J. Heat Transfer 131(2009)011701.

[4]H. Martin, Heat and mass transfer between impinging gas jets and solid surfaces in: James P.H. (Eds), Advances in Heat Transfer, Elsevier, New York, 1977: Vol. 13, pp.1-60.

[5]J.W. Baughn, S. Shimizu, Heat transfer measurements from a surface with uniform heat flux and an impinging jet, ASME J. Heat Transfer 111(4)(1989)1096-1098.

[6]D. Cooper, D.C. Jackson, B.E. Launder and G.X. Liao, Impinging jet studies for turbulence model assessmentłI. Flow-field experiments, Int. J. Heat Mass Transfer 36(10)(1993)2675-2684.

[7]L.F.G. Geers, M.J. Tummers and K. Hanjalic, Experimental investigation of impinging jet arrays, Exp. in Fluids 36(2004)946-958.

[8]H.B. Toda, O. Cabrit, K. Truffin, G. Bruneaux and F. Nicoud,Assessment of subgrid-scale models with a large-eddy simulation-dedicated experimental database: The pulsatile impinging jet in turbulent cross-flow, Phys. Fluids 26(2014)075108.

[9]X. Jiang, H. Zhao and K.H. Luo, Direct computation of perturbed impinging hot jets, Computers & Fluids 36(2)(2007)(259-272).

[10]T.J. Craft, L. Graham and B.E. Launder, Impinging jet studies for turbulence model assessment II. An examination of the performance of four turbulence models, Int. J. Heat Mass Transfer 36(10) (1993)2685-2697.

[11]T.S. Park, and H.J. Sung, Development of a near-wall turbulence model and application to jet impingement heat transfer, Int. J. Heat Fluid Flow 22(1) (2001)10-18.

[12]N. Zuckerman and N. Lior, Jet impingement heat transfer: physics, correlations, and numerical modeling, Advances in Heat Transfer 39(2006)565-631.

[13]M. Olsson, L. Fuchs, Large eddy simulations of a forced semiconfined circular impinging jet, Phys. Fluids 10(2)(1998)476-486.

[14]P.R. Voke, and S. Gao, Numerical study of heat transfer from an impinging jet, Int. J. Heat Mass Transfer 41(4-5) (1998)671-680.

[15]T. Cziesla, G. Biswas, H. Chattopadhyay and N. K. Mitra., Large-eddy simulation of flow and heat transfer in an impinging slot jet, Int. J. Heat Fluid Flow 22(5) (2001)500-508.

[16]M. Tsubokura, T. Kobayashi, N. Taniguchi and W.P. Jones, A numerical study on the eddy structures of impinging jets excited at the inlet, Int. J. Heat Fluid Flow, 24(4)(2003)500-511.

[17]F. Beaubert, S. Viazzo, Large eddy simulations of plane turbulent impinging jets at moderate Reynolds numbers, Int. J. Heat Fluid Flow 24(4) (2003)512-519.

[18]S. Rhea, M. Bini, M. Fairweather and W.P. Jones, RANS modelling and LES of a single-phase, impinging plane jet, Computers & Chemical Engineering 33(8) (2009)1344-1353.

[19]T. Hällqvist, Large eddy simulation of impinging jets with heat transfer, Technical Reports from Royal Institute of Technology, Department of Mechanics, S-100 44 Stockholm, Sweden 2006.

[20]M. Hadžiabdic, K. Hanjalic, Vortical structures and heat transfer in a round impinging jet, J. Fluid Mech. 596(2008)221-260.

[21]N. Uddin, S. O. Neumann, B. Weigand, and B.A. Younis, Large-eddy simulations and heat-flux modeling in a turbulent impinging jet, Numerical Heat Transfer, Part A 55(2009)906-930.

[22]F. Nicoud, H.B. Toda, O. Cabrit, S. Bose and J. Lee, Using singular values to build a subgrid-scale model for large eddy simulations, Phys. Fluids 23(2011)085106.

[23]M. Germano, U. Piomelli, P. Moin and W. Cabot, A dynamic subgrid-scale eddy viscosity model, Phys. Fluids A 3(7)(1991)1760-1765.

[24]A. Dewan, R. Dutta, and B. Srinivasan, Recent trends in computation of turbulent jet impingement heat transfer, Heat Transfer Engineering 33(4-5)(2012)447-460.

[25]U. Piomelli and J.H. Liu, Large-eddy simulation of rotating channel flows using a localized dynamic-model, Phys. Fluids 7(4)(1995)839-848.

[26]O. Métais, and M. Lesieur, New trend in large eddy simulation of turbulence. Annual Rev. Fluid Mech. 28(1996)45-82.

[27]Vreman, A. W. An eddy-viscosity subgrid-scale model for turbulent shear flow: algebraic theory and applications, Phys. Fluids 16(2004) 3670-3681.

[28]G. X. Cui, H.B. Zhou, Z. S. Zhang and L. Shao, A new subgrid eddy viscosity model and its application (in Chinese), Chinese J. Computer Physics 21(2004)289-293.

[29]G.X. Cui, C. X. Xu and Z. S. Zhang, Progress in large eddy simulation of turbulent flows (in Chinese), Acta Aerodynamica Sinica 22(2004) 121-129.

[30]Z.J. Zhu, H.X. Yang and T.Y. Chen, Numerical study of turbulent heat and fluid flow in a straight square duct at higher Reynolds numbers, Int. J. Heat Mass Transfer 53 (2010)356–364.

[31]Z.J. Zhu, J.L. Niu and Y.L. Li, Swirling-strength based large eddy simulation of turbulent flows around a single square cylinder at low Reynolds numbers, Appl. Math. Mech. -Engl. Ed., 35(8)(2014) 959-978.

[32]Z. Zhang, W. Chen, Z.J. Zhu and Y.L. Li, Numerical exploration of turbulent natural-convection in a differentially-heated air-filed square cavity at Ra $=5 \times 10^{9}$, Heat and Mass Transfer (2014) DOI 10.1007/s00231-014-1339-8.